

In the new basis, the action becomes

$$S = \int_0^\beta d\tau \int d^3x \bar{\psi}(\mathbf{x}) \left[\partial_\tau - \frac{\nabla^2}{2m} - \mu \right] \psi(\mathbf{x}).$$

The discrete and continuous measures, (12.133) and (12.134), respectively, are equivalent:

$$\prod_{\mathbf{k}, n} d\bar{c}_{\mathbf{k}n} dc_{\mathbf{k}n} \equiv \mathcal{D}[\bar{\psi}, \psi]$$

because the space of continuous functions $\psi(x)$ is spanned by a complete but discrete set of basis functions:

$$\psi(\mathbf{x}, \tau) = \frac{1}{\sqrt{\beta V}} \sum_{\mathbf{k}, n} c_{\mathbf{k}n} e^{i(\mathbf{k} \cdot \mathbf{x} - \omega_n \tau)}.$$

We can integrate over all possible functions $\psi(\mathbf{x}, \tau)$ by integrating over all values of the discrete vector $c_{\mathbf{k}n}$.

12.4.3 Gaussian path integral for fermions

For non-interacting fermions the action only involves bilinears of the Fermi fields, so the path integral is of Gaussian form and can always be evaluated. To discuss the most general case, we shall include source terms in the original Hamiltonian, writing

$$H(\tau) = \sum_{\lambda} [\epsilon_{\lambda} \hat{c}_{\lambda}^{\dagger} \hat{c}_{\lambda} - \bar{j}_{\lambda}(\tau) \hat{c}_{\lambda} - \hat{c}_{\lambda}^{\dagger} j_{\lambda}(\tau)],$$

where $\hat{c}_{\lambda}^{\dagger}$ is Schrödinger field that creates a fermion in the eigenstate with energy ϵ_{λ} . With source terms, the partition function becomes a *generating functional*,

$$Z[\bar{j}, j] = \text{Tr} \left[T \exp \left\{ - \int_0^\beta d\tau H(\tau) \right\} \right].$$

Derivatives of the generating functional generate the irreducible Green's functions of the fermions; for instance,

$$\frac{\delta \ln Z[\bar{j}, j]}{\delta \bar{j}(1)} = \langle c(1) \rangle \quad (12.135)$$

$$\frac{\delta^2 \ln Z[\bar{j}, j]}{\delta j(2) \delta \bar{j}(1)} = \langle T[c(1) c^{\dagger}(2)] \rangle - \langle c(2) \rangle \langle c^{\dagger}(1) \rangle, \quad (12.136)$$

where

$$\langle \dots \rangle = \frac{1}{Z[\bar{j}, j]} \text{Tr} \left[T \exp \left\{ - \int_0^\beta d\tau H(\tau) \right\} \dots \right].$$

Transforming to a path integral representation,

$$Z[\bar{j}, j] = \int \mathcal{D}[\bar{c}, c] e^{-S} \quad (12.137)$$

$$S = \int d\tau \left[\bar{c}(\tau) (\partial_\tau + \underline{h}) c(\tau) - \bar{j}(\tau) c(\tau) - \bar{c}(\tau) j(\tau) \right], \quad (12.138)$$

where $\underline{h}_{\alpha\beta} = \epsilon_{\alpha}\delta_{\alpha\beta}$ is the one-particle Hamiltonian. One can carry out functional derivatives on this integral without actually evaluating it. For example, we find that

$$\langle c(1) \rangle = \frac{1}{Z[\bar{j}, j]} \int \mathcal{D}[\bar{c}, c] c(1) e^{-S} \quad (12.139)$$

$$\langle T[c(1)c^\dagger(2)] \rangle = \frac{1}{Z[\bar{j}, j]} \int \mathcal{D}[\bar{c}, c] c(1)\bar{c}(2) e^{-S}. \quad (12.140)$$

Notice how the path integral automatically furnishes us with time-ordered expectation values.

Fortunately, the path integral is Gaussian, allowing us to use the general result obtained in Appendix 12D,

$$\int \prod_j d\bar{\xi}_j d\xi_j \exp[-\bar{\xi} \cdot A \cdot \xi + \bar{j} \cdot \xi + \bar{\xi} \cdot j] = \det A \exp[\bar{j} \cdot A^{-1} \cdot j]. \quad (12.141)$$

In the case considered here, $A = \partial_\tau + \underline{h}$, so we can do the integral to obtain

$$\begin{aligned} Z[\bar{j}, j] &= \int \mathcal{D}[\bar{c}, c] \exp \left[- \int_0^\beta d\tau \left[\bar{c}(\tau) (\partial_\tau + \underline{h}) c(\tau) - \bar{j}(\tau) c(\tau) - \bar{c}(\tau) j(\tau) \right] \right] \\ &= \det[\partial_\tau + \underline{h}] \exp \left[- \int_0^\beta d\tau d\tau' \bar{j}(\tau) \underline{G}[\tau - \tau'] j(\tau') \right], \end{aligned} \quad (12.142)$$

where

$$\underline{G}[\tau - \tau'] = -(\partial_\tau + \underline{h})^{-1}. \quad (12.143)$$

By differentiating (12.142) with respect to j and \bar{j} , we are able to identify

$$\left. \frac{\delta^2 \ln Z}{\delta j(\tau') \delta \bar{j}(\tau)} \right|_{\bar{j}, j=0} = (\partial_\tau + \underline{h})^{-1} = \langle c(\tau) c^\dagger(\tau') \rangle = -\underline{G}[\tau - \tau'], \quad (12.144)$$

so the inverse of the Gaussian coefficient in the action $-(\partial_\tau + \underline{h})^{-1}$ directly determines the imaginary-time Green's function of these non-interacting fermions. Higher-order moments of the generating functional provide a derivation of Wick's theorem.

From the partition function in (12.142), the free energy is then given by

$$F = -T \ln Z = -T \ln \det[\partial_\tau + \underline{h}] = -T \text{Tr} \ln[\partial_\tau + \underline{h}] = T \text{Tr} \ln[-G^{-1}],$$

where we have used the result $\ln \det[A] = \text{Tr} \ln[A]$.

To explicitly compute the free energy, it is useful to transform to Fourier components:

$$\begin{aligned} c_\lambda(\tau) &= \frac{1}{\sqrt{\beta}} \sum_n c_{\lambda n} e^{-i\omega_n \tau} \\ j_\lambda(\tau) &= \frac{1}{\sqrt{\beta}} \sum_n j_{\lambda n} e^{-i\omega_n \tau}. \end{aligned} \quad (12.145)$$

In this basis,

$$\begin{aligned} (\partial_\tau + \epsilon_\lambda) &\rightarrow (-i\omega_n + \epsilon_\lambda) \\ \underline{G} = -(\partial_\tau + \epsilon_\lambda)^{-1} &\rightarrow (i\omega_n - \epsilon_\lambda)^{-1}, \end{aligned} \quad (12.146)$$

so that

$$S = \sum_{\lambda,n} \left[[-i\omega_n + \epsilon_\lambda] \bar{c}_{\lambda n} c_{\lambda n} - \bar{j}_{\lambda n} c_{\lambda n} - \bar{c}_{\lambda n} j_{\lambda n} \right], \quad (12.147)$$

whereupon

$$\begin{aligned} \det[\partial_\tau + \underline{h}] &= \prod_{\lambda,n} (-i\omega_n + \epsilon_\lambda) \\ Z[\bar{j}, j] &= \prod_{\lambda,n} (-i\omega_n + \epsilon_\lambda) \exp \left[\sum_{\lambda,n} (-i\omega_n + \epsilon_\lambda)^{-1} \bar{j}_{\lambda n} j_{\lambda n} \right]. \end{aligned} \quad (12.148)$$

If we set $j = 0$ in Z , we obtain the free energy in terms of the fermionic Green's function:

$$F = -T \sum_{\lambda,n} \ln[-i\omega_n + \epsilon_\lambda].$$

As in the case of a single field, by replacing the Matsubara sum with a contour integral we obtain

$$F = \sum_{\lambda} \oint \frac{dz}{2\pi i} f(z) \ln[\epsilon_\lambda - z] \quad (12.149)$$

$$= -T \sum_{\lambda} \ln[1 + e^{-\beta\epsilon_\lambda}]. \quad (12.150)$$

If we differentiate Z with respect to its source terms, we obtain the Green's function:

$$-\frac{\delta^2 \ln Z}{\delta \bar{j}_{\lambda n} \delta j_{\lambda' n'}} = [\underline{G}]_{\lambda n, \lambda' n'} = \delta_{\lambda \lambda'} \delta_{nn'} \frac{1}{i\omega_n - \epsilon_\lambda}.$$

If we expand the logarithm of the partition function diagrammatically, then we get a series of linked-cluster diagrams,

$$\ln(Z/Z_0) = \text{diagram 1} + \text{diagram 2} + \text{diagram 3} + \text{diagram 4} + \dots, \quad (12.158)$$

where the point interaction is represented by the Feynman diagram

$$\text{diagram} = g\delta(\mathbf{1} - \mathbf{2}). \quad (12.159)$$

Rather than thinking of an instantaneous contact interaction, we can regard this diagram as the exchange of a force-carrying boson, writing the diagram as

$$\text{diagram} = \underbrace{(i)^2}_{\text{vertices}} \times \overbrace{-g\delta(\mathbf{1} - \mathbf{2})}^{-\langle T\phi(\mathbf{1})\phi(\mathbf{2}) \rangle}, \quad (12.160)$$

where the vertices $(-i)$ derive from an interaction $S'_I = \int_{\mathbf{x},\tau} \rho(x)\phi(x)$, between the fermions and the boson with imaginary-time Green's function

$$G(\mathbf{1} - \mathbf{2}) = -\langle T\phi(\mathbf{1})\phi(\mathbf{2}) \rangle = -g\delta(\mathbf{1} - \mathbf{2}). \quad (12.161)$$

But this implies that the exchange boson has a white-noise correlation function $\langle T\phi(\mathbf{1})\phi(\mathbf{2}) \rangle = \delta(\mathbf{1} - \mathbf{2})$: this kind of white-noise correlation is exactly what we expect for a field governed by a simple Gaussian path integral, where

$$\frac{\int D[\phi]\phi(\mathbf{1})\phi(\mathbf{2})e^{-S_\phi}}{\int D[\phi]e^{-S_\phi}} = g\delta(\mathbf{1} - \mathbf{2}), \quad (12.162)$$

with the Gaussian action

$$S_\phi = \int_{\mathbf{x}} \int_0^\beta d\tau \frac{\phi(x)^2}{2g}. \quad (12.163)$$

By adding $S_\phi + S'_I$ to the free fermion action, we can thus represent original point interaction by a fluctuating white-noise potential,

$$-\frac{g}{2}\rho(x)^2 \rightarrow \rho(x)\phi(x) + \frac{\phi(x)^2}{2g}. \quad (12.164)$$

If we now insert this transformed interaction into the action, the transformed path integral expression of the partition function becomes

$$Z = \int \mathcal{D}[\psi, \phi] \exp \left[- \int_{\mathbf{x},\tau} \left(\bar{\psi}(x)[\partial_\tau + \underline{h} + \phi(x)]\psi(x) + \frac{1}{2g}\phi(x)^2 \right) \right]. \quad (12.165)$$

where

$$\begin{aligned} S_E[\bar{\Delta}, \Delta] &= \sum_j \int d\tau \frac{\bar{\Delta}_j \Delta_j}{g} - \ln \det[\partial_\tau + \underline{h}_E[\bar{\Delta}, \Delta]] \\ &= \sum_j \int d\tau \frac{\bar{\Delta}_j \Delta_j}{g} - \text{Tr} \ln[\partial_\tau + \underline{h}_E[\bar{\Delta}, \Delta]]. \end{aligned} \quad (12.179)$$

effective action

Here we have made the replacement $\ln \det \rightarrow \text{Tr} \ln$. This quantity is called the *effective action* of the field Δ . The additional fermionic contribution to this action can profoundly change the distribution of the field Δ . For example, if S_E develops a minima around $\Delta = \Delta_o \neq 0$, then $\Delta = -A/g$ will acquire a vacuum expectation value. This makes the Hubbard–Stratonovich transformation an invaluable tool for studying the development of broken symmetry in interacting Fermi systems.

12.5.4 Generalizations to real variables and repulsive interactions

The method outlined in the previous section can also be applied to real fields. If we have an interaction between real fields, we can introduce a real white-noise field as follows:

$$H_I = -\frac{g}{2} \sum_j A_j^2 \rightarrow \sum_j \left\{ -\frac{g}{2} A_j^2 + \frac{q_j^2}{2g} \right\}. \quad (12.180)$$

Then, by redefining $q_j = Q_j + gA_j$, one obtains

$$-\frac{g}{2} \sum_j A_j^2 \rightarrow \sum_j \left\{ Q_j A_j + \frac{Q_j^2}{g} \right\}. \quad (12.181)$$

For example, we can use the Hubbard–Stratonovich transformation to replace an attractive interaction between fermions by a white-noise potential with variance g :

$$H_I = -\frac{g}{2} \sum_j (n_j)^2 \rightarrow \sum_{j\sigma} V_j n_j + \frac{V_j^2}{2g},$$

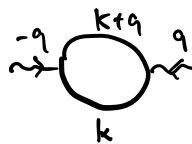
where $n_j = n_{j\uparrow} + n_{j\downarrow}$.

But what about repulsive interactions? These require a little more care, because we can't just change the sign of g in (12.181), for the integral over the white-noise fields will no longer be convergent. Instead, after introducing the dummy white-noise fields as before,

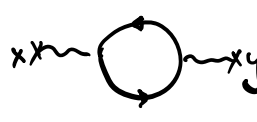
$$H_I = \frac{g}{2} A_j^2 \rightarrow \sum_j \left\{ \frac{g}{2} A_j^2 + \frac{q_j^2}{2g} \right\}, \quad (12.182)$$

$$\frac{\Delta S}{\beta V} = \frac{\Delta F}{V} = -\frac{1}{\beta V} \left[\sum \text{closed link diagrams in real space} \right]$$

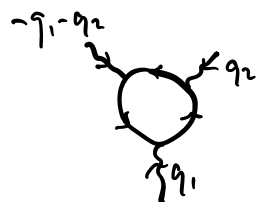
$$= - \sum \left[\text{closed link diagrams in momentum space.} \right]$$



$$= (-)^2 \frac{N}{2\beta V} \sum \phi_{-q} \phi_q G(k+q) G(k)$$



$$= - \frac{N}{2\beta V} \int d^4x d^4y \phi(x) \phi(y) G(x-y) G(y-x)$$



$$= - \frac{N}{3\beta V} \sum \phi_{-q_1-q_2} \phi_{q_1} \phi_{q_2} G(k+q_2) G(k+q_1) G(k)$$

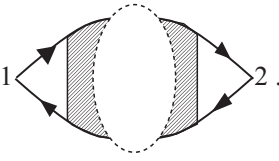


$$= - \frac{N}{3\beta V} \int d^4x d^4y d^4z \phi(x) \phi(y) \phi(z) G(x-z) G(z-y) G(y-x)$$

so that

$$\begin{aligned}
 i^2 \frac{\delta \ln S[\phi]}{\delta\phi(2)\delta\phi(1)} &= \frac{\langle \psi_0 | T\{S\rho(1)\rho(2)\} | \psi_0 \rangle}{S[\phi]} - \frac{\langle \psi_0 | S\rho(1) | \psi_0 \rangle}{S[\phi]} \frac{\langle \psi_0 | S\rho(2) | \psi_0 \rangle}{S[\phi]} \\
 &= \langle T\rho(1)\rho(2) \rangle - \langle \rho(1) \rangle \langle \rho(2) \rangle \\
 &= \langle T(\rho(1) - \langle \rho(1) \rangle)(\rho(2) - \langle \rho(2) \rangle) \rangle = \langle T\delta\rho(1)\delta\rho(2) \rangle. \quad (7.192)
 \end{aligned}$$

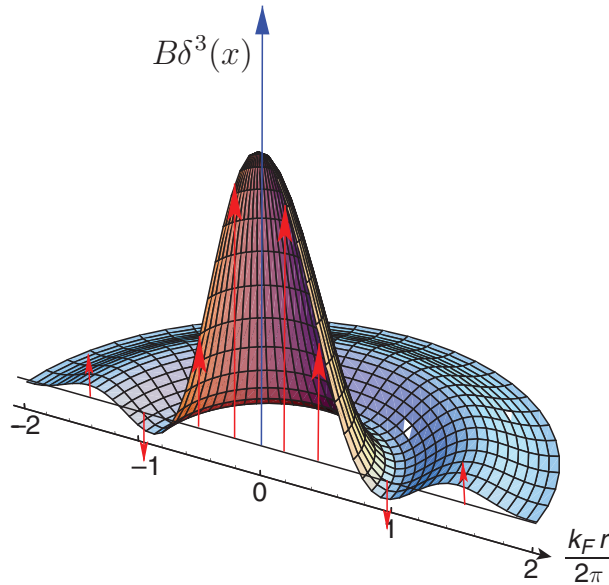
With this result and (7.82), we can now identify

$$\frac{\delta^2 \ln S[\phi]}{\delta\phi(2)\delta\phi(1)} = -\langle T\delta\rho(1)\delta\rho(2) \rangle = 1 \quad \text{---} \quad 2. \quad (7.193)$$


7.6.1 Magnetic susceptibility of non-interacting electron gas

One of the fundamental qualities of a Fermi liquid is its non-local response to an applied field. Suppose, for example, that one introduces a localized delta-function disturbance in the magnetic field, $\delta B_z(x) = B\delta^3(x)$. Since the fermions have a characteristic wavevector of order k_F , this local disturbance will “heal” over a length scale of order $l \sim 1/k_F$. Indeed, since the maximum wavevector for low-energy particle–hole excitations is sharply cut off at $2k_F$, the response produces oscillations in the spin density with a wavelength $\lambda = 2\pi/k_F$ that decay gradually from the site of the disturbance. These oscillations are called *Friedel oscillations* (Figure 7.5). In the case of the example just cited, the change in the spin density in response to the shift in the chemical potential is given by

$$\delta M(\vec{x}) = \chi_s(\vec{x})B, \quad (7.194)$$



Friedel oscillations in the spin density, in response to a delta-function disturbance in the magnetic field at the origin. These oscillations may be calculated from the Fourier transform of the Lindhard function.

Fig. 7.5

There are a number of important pieces of physics encoded in the above expression that deserve special discussion:

- Spin conservation. The total spin of the system is conserved, so that the application of a strictly uniform magnetic field to the fluid cannot change the total magnetization. Indeed, in keeping with this expectation, if we take $\vec{q} \rightarrow 0$ we find $\lim_{\vec{q} \rightarrow 0} \chi(\vec{q}, \nu) = 0$.
- Static susceptibility. When we take the limit $\nu \rightarrow 0$, we obtain the magnetization response to a spatially varying magnetic field. The static susceptibility is given by

$$\chi(\mathbf{q}) = 2\mu_B^2 \int_{\mathbf{k}} \frac{f_{\mathbf{k}} - f_{\mathbf{k}+\mathbf{q}}}{(\epsilon_{\mathbf{k}+\mathbf{q}} - \epsilon_{\mathbf{k}})}. \quad (7.203)$$

This response is finite, because the spins can always redistribute themselves in response to a non-uniform field. When we take the wavelength of the applied field to infinity, i.e. $q \rightarrow 0$, we recover the Pauli susceptibility:

$$\chi \rightarrow 2\mu_B^2 \int_{\mathbf{k}} \left(-\frac{df(\epsilon)}{d\epsilon} \right) = 2\mu_B^2 \int_{\mathbf{k}} \delta(\epsilon_{\mathbf{k}}) = 2\mu_B^2 N(0), \quad (7.204)$$

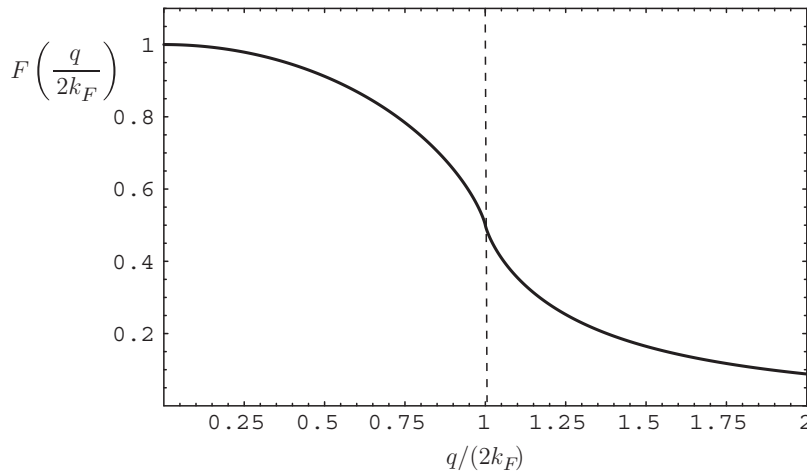
where $N(0) = \frac{mk_F}{2\pi^2}$ is the density of states per spin. The detailed momentum-dependent static susceptibility can be calculated (see Section 7.6.2), and is given by

$$\chi(\mathbf{q}) = 2\mu_B^2 N(0) F\left(\frac{q}{2k_F}\right) \\ F(x) = \frac{1}{4x}(1-x^2); \ln \left| \frac{1+x}{1-x} \right| + \frac{1}{2}. \quad (7.205)$$

The function $F(x)$ is known as the *Lindhard function* [5]; see Figure 7.6. It has the property that $F(0) = 1$, while $F'(x)$ has a weak logarithmic singularity at $|x| = 1$.

- Dissipation and the imaginary part of the susceptibility. The full dynamical spin susceptibility has both a real and an imaginary part, given by

$$\chi(\mathbf{q}, \nu) = \chi'(\mathbf{q}, \nu) + i\chi''(\mathbf{q}, \nu),$$



The Lindhard function. The Fourier transform of this function governs the magnetic response of a non-interacting metal to an applied field. Notice the weak singularity around $q/(2k_F) = 1$ that results from the match between the Fermi surface and the wavevector of the magnetic response.

Fig. 7.6

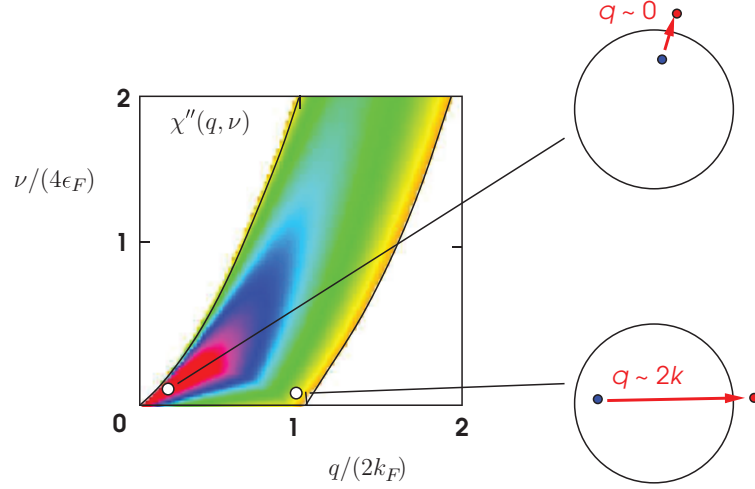


Fig. 7.7

Density plot of the imaginary part of the dynamical spin susceptibility calculated from (7.212), showing the band of width $2k_F$ that spreads up to higher energies. Excitations on the left side of the band correspond to low-momentum-transfer excitations of electrons from just beneath the Fermi surface to just above the Fermi surface. Excitations on the right-hand side of the band correspond to high-momentum-transfer processes, right across the Fermi surface.

where the imaginary part determines the dissipative part of the magnetic response. The dissipation arises because an applied magnetic field generates a cloud of electron–hole pairs which carry away the energy. If we use the Cauchy–Dirac relation $1/(x + i\delta) = P(1/x) - i\pi\delta(x)$ in (7.202), we obtain

$$\chi''(\mathbf{q}, \nu) = 2\mu_B^2 \int_{\mathbf{k}} \pi \delta[\nu - (\epsilon_{\mathbf{k}+\mathbf{q}} - \epsilon_{\mathbf{k}})] (f_{\mathbf{k}} - f_{\mathbf{k}+\mathbf{q}}). \quad (7.206)$$

This quantity defines the density of states of particle–hole excitations. The excitation energy of a particle–hole pair is given by

$$\epsilon_{\mathbf{k}+\mathbf{q}} - \epsilon_{\mathbf{k}} = \frac{q^2}{2m} + \frac{qk}{m} \cos \theta,$$

where θ is the angle between \mathbf{k} and \mathbf{q} . This quantity is largest when $\theta = 0$, $k = k_F$, and smallest when $\theta = \pi$, $k = k_F$, so that

$$\frac{q^2}{2m} + \frac{qk_F}{m} > \nu > \frac{q^2}{2m} - \frac{qk_F}{m}$$

defines a band of allowed wavevectors where the particle–hole density of states is finite, as shown in Figure 7.7. Outside this region, $\chi_0(\mathbf{q}, \nu)$ is purely real.

7.6.2 Derivation of the Lindhard function

The dynamical spin susceptibility

$$\chi(\mathbf{q}, \nu) = 2\mu_B^2 \int_{\mathbf{k}} \frac{f_{\mathbf{k}} - f_{\mathbf{k}+\mathbf{q}}}{(\epsilon_{\mathbf{k}+\mathbf{q}} - \epsilon_{\mathbf{k}} - \nu)} \quad (7.207)$$

can be rewritten as

$$\chi(\mathbf{q}, \nu) = 2\mu_B^2 \int_{\mathbf{k}} f_{\mathbf{k}} \left[\frac{1}{(\epsilon_{\mathbf{k}+\mathbf{q}} - \epsilon_{\mathbf{k}} - \nu)} + \frac{1}{(\epsilon_{\mathbf{k}-\mathbf{q}} - \epsilon_{\mathbf{k}} + \nu)} \right]. \quad (7.208)$$

- the hydrogen atom in N dimensions
- an electron gas with $N = 2S + 1$ spin components
- spin systems with spin S in the limit that S becomes large
- quantum chromodynamics with N rather than three colours.

In each of these cases, the limit $N \rightarrow \infty$ corresponds to a new kind of semiclassical limit, where certain variables cease to undergo quantum fluctuations. The parameter $1/N$ plays the role of an effective \hbar :

$$\frac{1}{N} \sim \hbar. \quad (7.213)$$

This does not, however, mean that quantum effects have been lost, merely that their macroscopic consequences can be lumped into certain semiclassical variables.

We shall now examine the second of these examples. The idea is to take an interacting Fermi gas where each fermion has $N = 2S + 1$ possible spin components. The interacting Hamiltonian is still written

$$H = \sum_{\mathbf{k}, \sigma} \epsilon_{\mathbf{k}} c_{\mathbf{k}\sigma}^{\dagger} c_{\mathbf{k}\sigma} + \frac{1}{2} \sum_{\mathbf{q}} V_{\mathbf{q}} c_{\mathbf{k}+\mathbf{q}\sigma}^{\dagger} c_{\mathbf{k}'-\mathbf{q}\sigma'}^{\dagger} c_{\mathbf{k}'\sigma'} c_{\mathbf{k}\sigma}, \quad (7.214)$$

but now the spin summations run over $N = 2S + 1$ values rather than just two. As N is made very large, it is important that both the kinetic energy and the interaction energy scale extensively with N . For this reason, the original interaction $V_{\mathbf{q}}$ is rescaled, writing

$$V_{\mathbf{q}} = \frac{1}{N} \mathcal{V}_{\mathbf{q}}, \quad (7.215)$$

where it is understood that, as $N \rightarrow \infty$, V is to be kept fixed. The idea is to now calculate quantities as an expansion in powers of $1/N$, and at the end of the calculation to give N the value of specific interest, in our case $N = 2$. For example, if we are interested in a Coulomb gas of spin- $\frac{1}{2}$ electrons, then we study the family of problems where

$$V_{\mathbf{q}} = \frac{1}{N} \frac{\tilde{e}^2}{q^2} = \frac{\mathcal{V}_{\mathbf{q}}}{N} \quad (7.216)$$

and $\tilde{e}^2 = 2e^2/\epsilon_0$. At the end, we set $N = 2$, boldly hoping that the key features of the solution around $N = 2$ will be shared by the entire family of models. In practice, this only holds true if the density of the electron gas is large enough to avoid instabilities such as the formation of Wigner crystal. For historical reasons, the approximation that appears in the large- N limit is called the *random phase approximation* (RPA), a method developed during the 1950s. The early version of the RPA was developed by David Bohm and David Pines [6], while its reformulation in a diagrammatic language was later given by Hubbard [7].² The large- N treatment of the electron gas recovers the RPA electron gas in a controlled approximation.

With the above substitution, the Feynman rules are unchanged, except that now we associate a factor $1/N$ with each interaction vertex. Before we start, however, there are a few preliminaries; in particular, we need to know how to handle long-range Coulomb

² A more detailed discussion of this early history can be found in the book by Nozières and Pines [8].

Thus by introducing a uniform positively charged background, we entirely remove the tadpole insertions.

Let us now examine how the fermions interact in this large- N Fermi gas. We can expand the effective interaction as follows:

$$iV_{eff}(q) = i\frac{\mathcal{V}_q}{N} + i\frac{\mathcal{V}_q}{N} \chi + i\frac{\mathcal{V}_q}{N} \chi^2 + i\frac{\mathcal{V}_q}{N} \chi^3 + \dots \quad (7.223)$$

The self-energy diagram for the interaction line is called a *polarization bubble*, and has the following diagrammatic expansion:

$$\chi = \text{O(N)} + \text{O(1)} + \text{O(1)} + \text{O(1/N)} + \dots = iN\chi(q). \quad (7.224)$$

By summing the geometric series that appears in (7.223), we obtain

$$V_{eff} = \frac{1}{N} \frac{\mathcal{V}(q)}{1 + \mathcal{V}(q)\chi(q)}. \quad (7.225)$$

This modification of the interaction by the polarization of the medium is an example of *screening*. In the large- N limit the higher-order Feynman diagrams for $\chi(q)$ are smaller by factors of $1/N$, so in the large- N limit these terms can be neglected, giving

$$i\chi(q)N = i\chi_0(q)N + O(1) = \text{bubble diagram} + O(1). \quad (7.226)$$

The large- N approximation, where we replace $\chi(q) \rightarrow \chi_0(q)$, is the random phase approximation (RPA).

In the case of a Coulomb interaction, the screened interaction becomes

$$V_{eff}(\mathbf{q}, \nu) = \frac{1}{N} \frac{\tilde{e}^2}{q^2 \epsilon_{RPA}(\mathbf{q}, \nu)}, \quad (7.227)$$

where we have identified the quantity

$$\epsilon_{RPA}(\mathbf{q}, \omega) = 1 + \mathcal{V}(q)\chi(q) = 1 + \frac{\tilde{e}^2}{q^2} \chi_0(q) \quad (7.228)$$

as the dielectric function of the charged medium. Notice how, in the interacting medium, the interaction between the fermions has become frequency-dependent, indicating that the interactions between the particles are now *retarded*. In our discussion of the Lindhard function, we showed that $\chi_0(q) = N(0)\mathcal{F}(q/(2k_F), \nu/(4\epsilon_F))$, where \mathcal{F} is the dimensionless Lindhard function and $N(0) = \frac{mk_F}{2\pi^2\hbar^2}$ is the density of states per spin at the Fermi surface, so we may write

$$\epsilon_{RPA}(\mathbf{q}, \omega) = 1 + \lambda \left(\frac{\mathcal{F}(\tilde{q}, \tilde{\nu})}{\tilde{q}^2} \right), \quad (7.229)$$

- The Bardeen–Pines interaction can be used to formulate an effective Hamiltonian for the low-energy physics of jellium, known as the *Bardeen–Pines Hamiltonian*:

$$H_{BP} = \sum_{\mathbf{k}\sigma} \epsilon_{\mathbf{k}} c_{\mathbf{k}\sigma}^{\dagger} c_{\mathbf{k}\sigma} + \frac{1}{2} \sum_{\mathbf{k}, \mathbf{k}'} V_{\text{eff}}(\mathbf{q}, \epsilon_{\mathbf{k}} - \epsilon_{\mathbf{k}'}) c_{\mathbf{k}-\mathbf{q}\sigma}^{\dagger} c_{\mathbf{k}'+\mathbf{q}\sigma'}^{\dagger} c_{\mathbf{k}'\sigma'} c_{\mathbf{k}\sigma}. \quad (7.256)$$

Bardeen–Pines Hamiltonian

The Bardeen–Pines Hamiltonian is the predecessor of the Bardeen–Cooper–Schrieffer (BCS) model, and demonstrates that, while the intrinsic electron–electron interaction is repulsive, “overscreening” by the lattice causes it to develop a retarded attractive component (see Exercise 7.8).

7.7.4 Zero-point energy of the RPA electron gas

Let us now examine the linked-cluster expansion of the ground state energy. Without the tadpole insertions, the only non-zero diagrams are then

$$\begin{aligned} \frac{\Delta E}{V} = & \left(\text{diagram 1} + \text{diagram 2} + \text{diagram 3} + \text{diagram 4} + \dots \right) \\ & + \left(\text{diagram 5} + \text{diagram 6} + \dots \right) + \left(\text{diagram 7} + \dots \right) + \dots \end{aligned} \quad (7.257)$$

$\text{diagram 1} \sim \text{diagram 2} \sim \text{diagram 3} \sim \text{diagram 4} \sim \text{diagram 5} \sim \text{diagram 6} \sim \text{diagram 7} \sim \text{diagram 8} \sim \text{diagram 9} \sim \text{diagram 10} \sim \text{diagram 11} \sim \text{diagram 12} \sim \text{diagram 13} \sim \text{diagram 14} \sim \text{diagram 15} \sim \text{diagram 16} \sim \text{diagram 17} \sim \text{diagram 18} \sim \text{diagram 19} \sim \text{diagram 20} \sim \text{diagram 21} \sim \text{diagram 22} \sim \text{diagram 23} \sim \text{diagram 24} \sim \text{diagram 25} \sim \text{diagram 26} \sim \text{diagram 27} \sim \text{diagram 28} \sim \text{diagram 29} \sim \text{diagram 30} \sim \text{diagram 31} \sim \text{diagram 32} \sim \text{diagram 33} \sim \text{diagram 34} \sim \text{diagram 35} \sim \text{diagram 36} \sim \text{diagram 37} \sim \text{diagram 38} \sim \text{diagram 39} \sim \text{diagram 40} \sim \text{diagram 41} \sim \text{diagram 42} \sim \text{diagram 43} \sim \text{diagram 44} \sim \text{diagram 45} \sim \text{diagram 46} \sim \text{diagram 47} \sim \text{diagram 48} \sim \text{diagram 49} \sim \text{diagram 50} \sim \text{diagram 51} \sim \text{diagram 52} \sim \text{diagram 53} \sim \text{diagram 54} \sim \text{diagram 55} \sim \text{diagram 56} \sim \text{diagram 57} \sim \text{diagram 58} \sim \text{diagram 59} \sim \text{diagram 60} \sim \text{diagram 61} \sim \text{diagram 62} \sim \text{diagram 63} \sim \text{diagram 64} \sim \text{diagram 65} \sim \text{diagram 66} \sim \text{diagram 67} \sim \text{diagram 68} \sim \text{diagram 69} \sim \text{diagram 70} \sim \text{diagram 71} \sim \text{diagram 72} \sim \text{diagram 73} \sim \text{diagram 74} \sim \text{diagram 75} \sim \text{diagram 76} \sim \text{diagram 77} \sim \text{diagram 78} \sim \text{diagram 79} \sim \text{diagram 80} \sim \text{diagram 81} \sim \text{diagram 82} \sim \text{diagram 83} \sim \text{diagram 84} \sim \text{diagram 85} \sim \text{diagram 86} \sim \text{diagram 87} \sim \text{diagram 88} \sim \text{diagram 89} \sim \text{diagram 90} \sim \text{diagram 91} \sim \text{diagram 92} \sim \text{diagram 93} \sim \text{diagram 94} \sim \text{diagram 95} \sim \text{diagram 96} \sim \text{diagram 97} \sim \text{diagram 98} \sim \text{diagram 99} \sim \text{diagram 100} \sim \dots$

These diagrams are derived from the zero-point fluctuations in charge density, which modify the ground state energy $E \rightarrow E_0 + E_{zp}$. We shall select the leading contribution,

$$\frac{E_{zp}}{V} = \text{diagram 1} + \text{diagram 2} + \text{diagram 3} + \text{diagram 4} + \dots \quad (7.258)$$

$\text{diagram 1} \sim \text{diagram 2} \sim \text{diagram 3} \sim \text{diagram 4} \sim \text{diagram 5} \sim \text{diagram 6} \sim \text{diagram 7} \sim \text{diagram 8} \sim \text{diagram 9} \sim \text{diagram 10} \sim \text{diagram 11} \sim \text{diagram 12} \sim \text{diagram 13} \sim \text{diagram 14} \sim \text{diagram 15} \sim \text{diagram 16} \sim \text{diagram 17} \sim \text{diagram 18} \sim \text{diagram 19} \sim \text{diagram 20} \sim \text{diagram 21} \sim \text{diagram 22} \sim \text{diagram 23} \sim \text{diagram 24} \sim \text{diagram 25} \sim \text{diagram 26} \sim \text{diagram 27} \sim \text{diagram 28} \sim \text{diagram 29} \sim \text{diagram 30} \sim \text{diagram 31} \sim \text{diagram 32} \sim \text{diagram 33} \sim \text{diagram 34} \sim \text{diagram 35} \sim \text{diagram 36} \sim \text{diagram 37} \sim \text{diagram 38} \sim \text{diagram 39} \sim \text{diagram 40} \sim \text{diagram 41} \sim \text{diagram 42} \sim \text{diagram 43} \sim \text{diagram 44} \sim \text{diagram 45} \sim \text{diagram 46} \sim \text{diagram 47} \sim \text{diagram 48} \sim \text{diagram 49} \sim \text{diagram 50} \sim \text{diagram 51} \sim \text{diagram 52} \sim \text{diagram 53} \sim \text{diagram 54} \sim \text{diagram 55} \sim \text{diagram 56} \sim \text{diagram 57} \sim \text{diagram 58} \sim \text{diagram 59} \sim \text{diagram 60} \sim \text{diagram 61} \sim \text{diagram 62} \sim \text{diagram 63} \sim \text{diagram 64} \sim \text{diagram 65} \sim \text{diagram 66} \sim \text{diagram 67} \sim \text{diagram 68} \sim \text{diagram 69} \sim \text{diagram 70} \sim \text{diagram 71} \sim \text{diagram 72} \sim \text{diagram 73} \sim \text{diagram 74} \sim \text{diagram 75} \sim \text{diagram 76} \sim \text{diagram 77} \sim \text{diagram 78} \sim \text{diagram 79} \sim \text{diagram 80} \sim \text{diagram 81} \sim \text{diagram 82} \sim \text{diagram 83} \sim \text{diagram 84} \sim \text{diagram 85} \sim \text{diagram 86} \sim \text{diagram 87} \sim \text{diagram 88} \sim \text{diagram 89} \sim \text{diagram 90} \sim \text{diagram 91} \sim \text{diagram 92} \sim \text{diagram 93} \sim \text{diagram 94} \sim \text{diagram 95} \sim \text{diagram 96} \sim \text{diagram 97} \sim \text{diagram 98} \sim \text{diagram 99} \sim \text{diagram 100} \sim \dots$

The n th diagram in this series has a symmetry factor $p = 2n$, and a contribution $(-\chi_0(q)\mathcal{V}(q))^n$ associated with the n polarization bubbles and interaction lines. The energy per unit volume associated with this series of diagrams is thus

$$E_{zp} = i \sum_{n=1}^{\infty} \frac{1}{2n} \int \frac{d^4q}{(2\pi)^4} (-\chi_0(q)\mathcal{V}(q))^n. \quad (7.259)$$